Effect of water nanoconfinement on the dynamic properties of paramagnetic colloidal complexes

PCCP

ARTICLE TYPE

Cite this: DOI: 00.0000/xxxxxxxxxx

Effect of water nanoconfinement on the dynamic properties of paramagnetic colloidal complexes

Luca Bergamasco,[a] Matteo Morciano,[a] and Matteo Fasano[a,*]

Received Date
Accepted Date

DOI: 00.0000/xxxxxxxxxx

The anomalous behavior of confined water at the nanoscale has remarkable implications in a number of nanotechnological applications. In this work, we analyze the effect of water self-diffusion on the dynamic properties of a solvated gadolinium-based paramagnetic complex, typically used for contrast enhancement in magnetic resonance imaging. In particular, we examine the effect of silica-based nanostructures on water behavior in the proximity of the paramagnetic complex via atomistic simulations, and interpret the resulting tumbling dynamics in the light of the local solvent modification based on the Lipari-Szabo formalism and of the fractional Stokes-Einstein relation. It is found that the local water confinement induces an increased "stiffness" on the outer sphere of the paramagnetic complex, which eventually reduces its tumbling properties. These model predictions are found to explain well the relaxivity enhancement observed experimentally by confining paramagnetic complexes into porous nanocontructs, and thus offer mechanistic guidelines to design improved contrast agents for imaging applications.

Introduction

Confined molecular liquids have peculiar properties which are significantly different from those in bulk conditions.[1–3] Thorough understanding of these features is key to enable optimization of nanoscale devices for a number of different applications, such as membrane separation for desalination and filtration, oil and gas production, energy conversion and storage or DNA sequencing.[4–11] Bioengineering and nanomedicine are certainly among those fields where the anomalous behavior of nanoconfined liquids, water in particular, can be exploited to improve controlled drug delivery for therapeutics and imaging techniques.[12–16]

Magnetic Resonance Imaging (MRI) is a technique used in the medical field, which allows to obtain accurate images of biological matter in the human body. MRI relies on the principles of the Nuclear Magnetic Resonance (NMR), which is a spectroscopic phenomenon produced by the interaction between hydrogen protons immersed in a static magnetic field and a second oscillating external magnetic field.[17] Upon application of a transverse radio frequency pulse, protons are perturbed and the subsequent process through which they return to their original initial state is referred to as *relaxation*. Two concurrent processes, namely the longitudinal relaxation (T_1-decay) and the transverse relaxation (T_2-decay) are monitored to generate an MR image. In particular, T_1 is the time constant for the physical processes responsible for the relaxation of the components of the nuclear spin magnetization vector $\mathbf{M}$ parallel to the applied external magnetic field $\mathbf{B}_0$, whereas T_2 relaxation affects the components of $\mathbf{M}$ perpendicular to $\mathbf{B}_0$. The local variation in relaxation, generating the image contrast, arises from the different local proton densities and from the chemical and physical nature of the tissues which are object of the imaging analysis.[18]

Contrast agents allow to improve the contrast between healthy and pathological tissues in MRI scans. Complexes based on paramagnetic materials, such as lanthanide ions or iron oxides, have the ability to decrease the relaxation times of the nearby protons via dipolar interactions; thus, they have received remarkable attention as potential contrast agents.[17] In this view, however, the contrast enhancement in the proximity of the paramagnetic complexes is strongly influenced by the local dynamics and diffusion of the water molecules[19], which may in turn be sensitive to the effect of nearby hard/soft interfaces. For gadolinium (Gd^{3+}) paramagnetic metal complexes for example, the Solomon-Bloembergen-Morgan (SBM) theory would predict a change in the longitudinal relaxivity r_1 of the complex following a variation in the relative translational diffusion time of the water molecules surrounding the complex, and in the residence lifetime of the water molecules bound to the complex.[17] Similarly, for magnetic nanoparticles such as superparamagnetic iron oxide nanoparticles (SPIOs), an increase in the diffusion time of the water molecules (*i.e.* a decrease in the local water self-diffusion coefficient) would enhance the r_2 transverse relaxivity.[20] Therefore, the modulation and precise control of the diffusion properties of the water molecules in the vicinity of the paramagnetic complex plays an

[a] *Department of Energy, Politecnico di Torino, Corso Duca degli Abruzzi 24, 10129 Torino (Italy).* * *E-mail: matteo.fasano@polito.it*

† Electronic Supplementary Information (ESI) available.

important role for fine tuning of the imaging performance.[21] An extensive overview with a recent discussion on the topic can be found in Reference[22].

It has been also demonstrated that the covalent attachment of the complex through the (3-aminopropyl) triethoxysilane to the surface of either Silicon Mesoporous Particles (SiMPs) or nonporous SiO_2 Particles (SiP), used for delivery of therapeutic and imaging agents, have a different effect on increasing the relaxivity values of the Gd^{3+} ions when compared to free Gd(DOTA) complex in aqueous solution.[23] The analyzed SiMPs were characterized by either ≈ 50 nm (HP) or 5–10 nm (SP) nanopore diameters. The experiments showed that, starting from the r_1 value for Gd(DOTA) in bulk conditions (about 4 $mM^{-1}s^{-1}$), r_1 increases to 16.8 ± 1.9 $mM^{-1}s^{-1}$ for the SiMP-SP particles, to 13.7 ± 0.6 $mM^{-1}s^{-1}$ for SiMP-HP particles and to 8.09 ± 2.1 $mM^{-1}s^{-1}$ for SiP.[23] The given increases in r_1 values are expected due to the anchoring of Gd(DOTA) to the slowly tumbling nanoparticles. Moreover, the latter increase is observed to be function of the porosity of the nanoparticles, since the diffusion of water molecules tends to be different according to the pore size.[3] In fact, SiMPs-SP with the smaller pore size of 5–10 nm result in higher r_1 values when compared to SiMPs-HP with pore size of ≈ 50 nm, and SiO_2 leads to the smallest increase due to the nonporous structure of the nanoparticles. The observed relaxivity enhancements may be attributed to the concurrent increase of both diffusion (τ_D) and tumbling (τ_R) times of the Gd(DOTA) complex, as a result of the confined conditions experienced by the water molecules in the proximity of the SiMP/SiP surfaces.

In this work, we propose an original mechanistic interpretation of the relaxivity enhancement of Gd(DOTA) bonded to solid surfaces by studying the peculiar transport properties of nanoconfined water. Molecular Dynamics (MD) simulations are analyzed in the light of the Lipari-Szabo formalism, a previously reported scaling law for the self-diffusion coefficient of water in confined conditions,[3] and the fractional version of the Stokes-Einstein relation. The resulting bottom-up model of Gd(DOTA) relaxivity is found to be in good agreement with previously reported experiments.

Methods

Geometry

The performed MD study takes inspiration from the experimental setup analyzed in Reference[23], namely the paramagnetic complex of the Gd(DOTA) contrast agent (Dotarem©), chemically bonded to mesoporous (SiMP) or nonporous (SiP) silicon-based particles.

Gd(DOTA) is a paramagnetic complex made of a gadolinium ion (Gd^{3+}) enclosed in 1,4,7,10-tetraazacyclododecane-1,4,7,10-tetraacetic acid (DOTA), which serves for stability and biocompatibility purposes. The Gd(DOTA) structure (Figure 1a) has been already previously studied and fully characterized by experiments and atomistic simulations.[24,25]

A silica slab (2.1 x 2.5 x 1.5 nm^3, periodic along the x and y directions) is chosen for mimicking the surface of the SiMP or SiP nanostructure. The atomic coordinates of the solid wall are generated starting from a silica (SiO_2) crystal[26], whereas silanol groups are added as a surface functionalization. The Gd(DOTA) complex is then bonded to the silica surface (Figure 1b) by means of the harmonic potential $U_{Si-Gd(DOTA)} = k(r_{OC} - b)^2$, where r_{OC} is the distance between the surface oxygen of the silica wall in correspondence of its barycenter and a carbon atom of DOTA, k the harmonic constant (400000 kJ mol^{-1} nm^{-2}) and b the equilibrium length of the bond. Note that k has been chosen to lie in the range of typical values of harmonic constants for the bonded interactions in organic compounds[27], whereas b mimics the length of a chain chemically bonding the contrast agent to a bigger particle, as in the case of complexes made out of APTES (aminosilane chain approximately 1 nm long), Gd(DOTA) (contrast agent) and SiP/SiMP (micrometer-sized particles), as shown in Figure 1c.[23]

The Gd(DOTA) and the silica structures are then solvated by TIP3P water model[28], which has been proved to better simulate tumbling properties of Gd(DOTA) at room temperature.[25,29] After solvation, the size of the computational box employed to simulate the free tumbling of Gd(DOTA) in water is 4 x 4 x 4 nm^3, whereas the ones to study the tumbling motion of Gd(DOTA) bounded to the solid wall are 2.5 x 2.1 x 10.2 nm^3. Since the solid wall is 1.5 nm thick, the latter setup mimics a nanoconfined water cavity with 8.5 nm thickness that allows to recover bulk water conditions at the center.[3]

Different definitions for the Gd(DOTA)-silica relative distances are adopted (see Figure 1d). In particular, b is the length of the DOTA-silica covalent bond; d_{min} is the average minimum distance between the silica wall and the Gd(DOTA) atoms during the simulation; $r_{Gd(DOTA)}$ is the average radius of the Gd(DOTA) compound ($\cong 0.5$ nm), and $d = d_{min} + r_{Gd(DOTA)}$ is the normal distance (*i.e.* evaluated along z axis) between the silica surface and the Gd(DOTA) barycenter. A detailed overview of the simulated configurations is available in the ESI†, S1.

Force field

Two types of interactions are considered in the MD simulations: i) bonded interactions, among the atoms forming the silica wall and DOTA; ii) nonbonded interactions, among the atoms of the silica wall, the Gd(DOTA) and water.

In the silica and DOTA structures, the bonded interactions are modeled by means of two harmonic terms, which reproduce the stretch and angle oscillations around the equilibrium positions of the solid structures. Bonded parameters of silica and DOTA are taken from Reference[30] and[31], respectively.

Nonbonded interactions among the silica, water and Gd(DOTA) atoms (consisting in both van der Waals and electrostatic interactions) are also taken into account through: (i) a 12-6 Lennard-Jones term, with mixed parameters chosen according to Lorentz-Berthelot combination rules; and (ii) a Coulomb term, which takes into account the interactions between the partial charges of the structures and the water dipole. Nonbonded parameters of silica are reported in Reference[32]; optimized partial charges for Gd(DOTA) are available in Reference[33], whereas Lennard-Jones parameters are reported in References[25] and[31]. Introducing bonds of crystallographic length between the Gd ion and the coordination sphere avoids undesired behaviors during the sim-

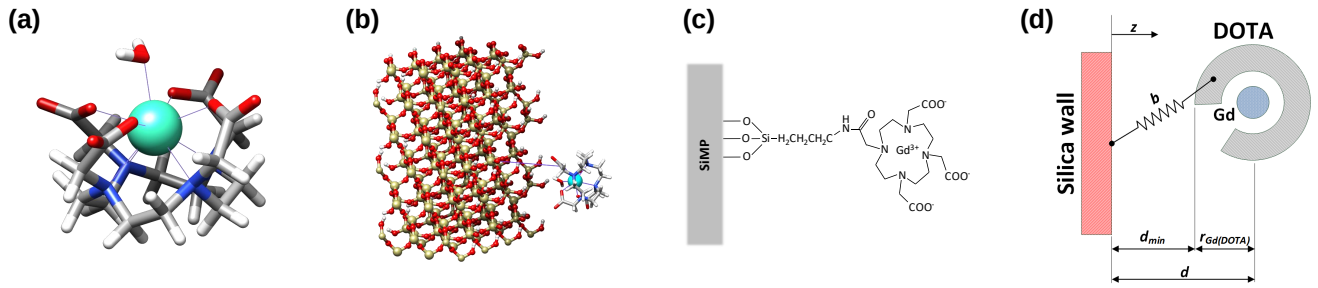

Fig. 1 Overview of the analyzed Gd(DOTA) configurations. (a) Gd(DOTA) geometry used in the molecular dynamics simulations. The purple lines represent the interactions between a Gd^{3+} ion and the atoms of the first coordination sphere. (b) Gd(DOTA) and the silica wall geometry in the molecular dynamics simulations. Gd(DOTA) is covalently bonded to a silica surface (e.g. surface of mesoporous silicon nanoconstructs or particles). (c) Possible chemical bonding between Gd(DOTA) and a solid surface via (3-aminopropyl) triethoxysilane (APTES) groups, as tested in Reference [23]. (d) Schematic representation of the Gd(DOTA)/silica wall complex and their reciprocal distances.

ulation (e.g. the departure of the inner-sphere water molecule). This treatment is justified because the Gd(DOTA) complex can be considered as stable on the molecular dynamics time scale. [29]

Simulation protocol

MD simulations are carried out using GROMACS [34,35], while rendering pictures are made with UCSF Chimera. [36] Lennard-Jones potentials are treated with a twin-range cut-off modified by a shift function (1.0 nm cut-off distance), whereas the Particle-Mesh Ewald (PME) algorithm [37] with 1.2 nm real-space cutoff and 0.12 nm reciprocal space gridding is chosen for electrostatic interactions. Simulations are carried out with a leap-frog algorithm and time step $\Delta t = 0.5$ fs, while periodic boundary conditions are applied along x, y and z directions. Long range dispersion corrections are applied to avoid energy artifacts. After that, the solvated geometry is energy minimized and a K^+ counterion is added to neutralize the system, the system is initialized by a Maxwellian distribution of velocities and coupled to a Berendsen thermostat at 300 K for 10 ns (time constant $\tau = 0.2$ ps) [38], until the energies of the system relax to steady state. Afterwards, simulations are continued up to 10 ns in NPT ensemble, by introducing Nosé-Hoover thermostat (300 K and $\tau = 0.2$ ps) [39,40] and Parrinello-Rahman barostat (1 bar and $\tau = 0.5$ ps). [41] The steady state is considered as achieved when the measured quantities (e.g. tumbling times, energies, relative distances) tend to asymptotic values (see ESI†, S2).

The Lipari-Szabo model-free approach

The complex motion of an atomic bond A-B can be decomposed in two simpler components: translational and rotational motion. [42] The Lipari and Szapo theory focuses on the rotational component of motion (*i.e.* tumbling), and it allows to fully represent complex tumbling (e.g. A-B could rotate around some point in the center of the bond, or swing around like a clock hand, or wobble at the ends) by means of a few characteristic time constants.

Let us first consider the atomic bond A-B in a freely tumbling molecule, that is, which is not restrained in its motion. A generic autocorrelation function $C_f(t)$ for a property $f(t)$ is defined as

$$C_f(t) = \langle f(\xi) f(\xi + t) \rangle_\xi, \quad (1)$$

where on the right-hand side an average over multiple time origins ξ is considered via the operator $\langle \ldots \rangle_\xi$. In this case, the Rotational Autocorrelation Function - RACF ($C(t)$) of a vector $p = \overrightarrow{AB}$ is the correlation between the orientation of one (or more) bond vectors of the molecule.

If the A-B bond belongs to a free molecule (e.g. Gd(DOTA) in water in Figure 1a), the Lipari and Szapo theory states that its tumbling motion can be characterized by τ_R, namely the characteristic tumbling (or rotational correlation) time of the system. This characteristic time can be evaluated from the RACF considering that

$$C(t) = \exp\left(-\frac{t}{\tau_R}\right). \quad (2)$$

However, if the A-B bond belongs to a molecule that is part of a more complex structure (e.g. Gd(DOTA) bonded to a SiMP/SiP), its tumbling is originated by two distinct motions: a local (*i.e.* A-B tumbling within the molecule) and a global (*i.e.* tumbling of the overall structure) motion. Therefore, a second correlation function – $C_E(t)$ or extra correlation function – is introduced, for taking into account the relative motion between the A-B bond and the overall structure (e.g. tumbling motion of Gd(DOTA) with respect to the SiMP/SiP):

$$C_E(t) = S^2 + \left(1 - S^2\right) \exp\left(-\frac{t}{\tau_E}\right), \quad (3)$$

where τ_E is the extra correlation time and S^2 the order parameter, which quantifies the coupling between the local and global motions. [42,43] If the coupling between the molecule where A-B bond is situated and the overall complex is absolutely rigid, then $S^2 = 1$, namely a 100% chance of finding A-B bond in the same position at any instant; on the other hand, if the coupling is completely flexible, then $S^2 = 0$ and the form of Equation 2 is recovered. Equation 2 can be adopted again to describe the tumbling of the overall structure (e.g. tumbling motion of SiMP/SiP) in terms of

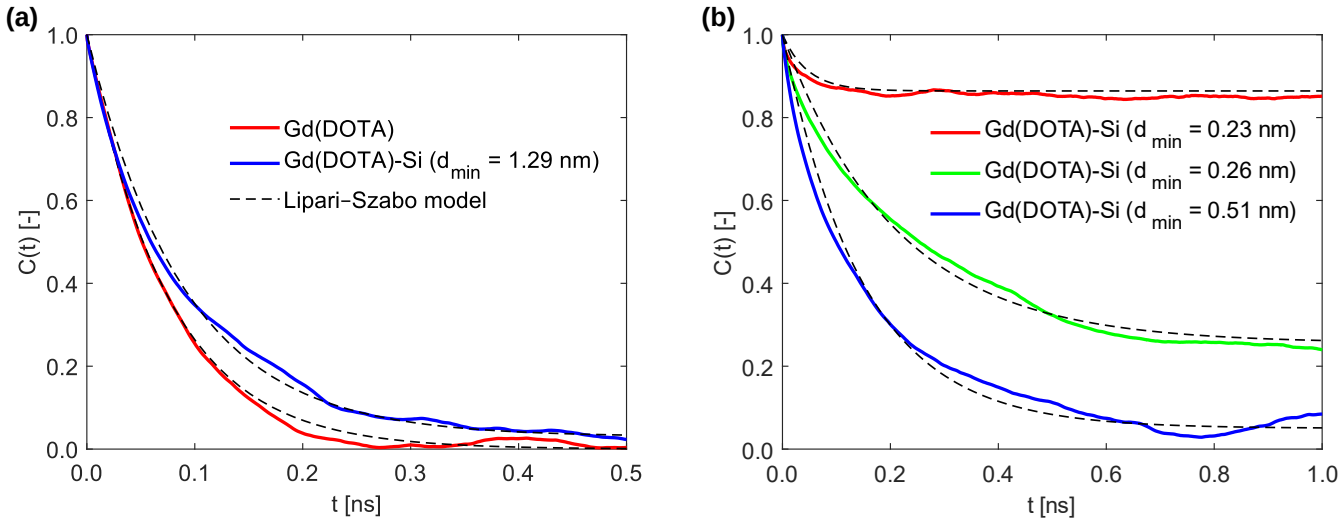

Fig. 2 Autocorrelation functions of Gd(DOTA) coordination sphere – as obtained from MD simulations – are depicted and fitted by proper Lipari-Szapo models. (a) Gd(DOTA) in bulk water (red solid line: MD results; black dashed line: Lipari-Szapo model fitting $C(t)=\exp(-t/\tau_R)$, R^2=0.99); Gd(DOTA) bonded to a silica wall with $d_{min}=1.29$ nm (blue solid line: MD results; black dashed line: Lipari-Szapo model fitting $C(t)=S^2+(1-S^2)\exp(-t/\tau_E)$, R^2=0.98). (b) Gd(DOTA) bonded to a silica wall with $d_{min}=0.23$ nm (red solid line), $d_{min}=0.26$ nm (green solid line) and 0.51 nm (blue solid line), respectively. MD results are fitted by Lipari-Szapo model (black dashed lines) $C(t)=S^2+(1-S^2)\exp(-t/\tau_E)$ with R^2 values of 0.85, 0.94 and 0.96, respectively.

a molecular correlation time τ_M as:

$$C_M(t)=\exp\left(-\frac{t}{\tau_M}\right). \quad (4)$$

Finally, if the extra and molecular motions are independent from each other, the A-B tumbling can be fully described as $C_E(t)C_M(t)$, which yields:

$$C(t)=S^2\exp\left(-\frac{t}{\tau_M}\right)+\left(1-S^2\right)\exp\left(-\frac{t}{\tau_T}\right), \quad (5)$$

where the characteristic time τ_T relates molecular and extra correlation times as $\tau_T^{-1}=\tau_M^{-1}+\tau_E^{-1}$. Clearly, only $C_E(t)$ can be extracted from the MD configuration in Figure 1b, since the micrometer-sized SiMP/SiP should be mimicked as a steady wall in the considered nanometer-sized domain.

The Lipari-Szapo formalism has been successfully applied for analyzing Nuclear Magnetic Resonance relaxation data in terms of tumbling and rotational motion of proteins[44,45], RNA[43], sugars or micellized surfactants[46], and it is recognized as a simple but accurate form of the spectral density function describing the motion of NMR probes.[47]

Results

Tumbling time

The characteristic tumbling motion of the paramagnetic complex strongly influences its relaxivity, as it characterizes the interaction speed with the surrounding protons. Therefore, in order to enhance the relaxivity, a typical strategy relies on the increase of the rotational correlation time.[19]

Atomistic simulations have been widely used to estimate the characteristic rotational correlation time of biomolecules or organic/inorganic particles.[19,25,29,33,44] Indeed, from MD trajectories, it is possible to calculate the RACF of selected vectors (*i.e.* atomic bonds) in a solvated molecule, which can be used to estimate τ_R or τ_E using the Lipari-Szapo approach. Here, MD simulations are performed to estimate the tumbling time of the Gd(DOTA) complex in two different conditions: (i) Gd(DOTA) complex solvated in bulk water (Figure 1a); (ii) solvated Gd(DOTA) complex bonded to a silica wall (Figure 1b), being b the imposed equilibrium distance for the silica-DOTA bond (Figure 1d). Different values of b are analyzed, namely 0.4, 0.5, 0.8, 1.0, 2.0, 3.0 nm (see ESI†, S1 for further details of the tested configurations), in order to assess the effect of the silica-DOTA bond length on the Gd(DOTA) tumbling motion.

In order to obtain better statistics, for each of the considered configurations we: i) perform multiple simulations with random initial velocities; ii) evaluate multiple RACFs for each repetition; iii) obtain the final RACF and the averaged values of the characteristic tumbling time per configuration. In general, the RACF can be evaluated for each trajectory as[37]

$$C(t)=\int_0^\infty P_2\left(\frac{p(\xi)\cdot p(\xi+t)}{\|p(\xi)\|\,\|p(\xi+t)\|}\right)d\xi, \quad (6)$$

with P_2 being the second-order Legendre polynomial. In our case, the RACF for the i-th trajectory is obtained as[33]

$$C_i(t)=\frac{1}{M}\sum_{j=0}^{M-1}\left[\frac{1}{9}\sum_{k=1}^{9}\left(\int_{t_{b,j}}^{t_{e,j}}P_2\left(\frac{p_k(\xi)\cdot p_k(\xi+t)}{\|p_k(\xi)\|\,\|p_k(\xi+t)\|}\right)d\xi\right)\right], \quad (7)$$

with k being the index of the nine inner-sphere coordination vectors of the of Gd atom, and j the index of the discrete time intervals (Δt) for the integration, defined as

$$t_{b,j}=j\frac{\Delta t}{M},\quad t_{e,j}=t_{b,j}+\Delta t. \quad (8)$$

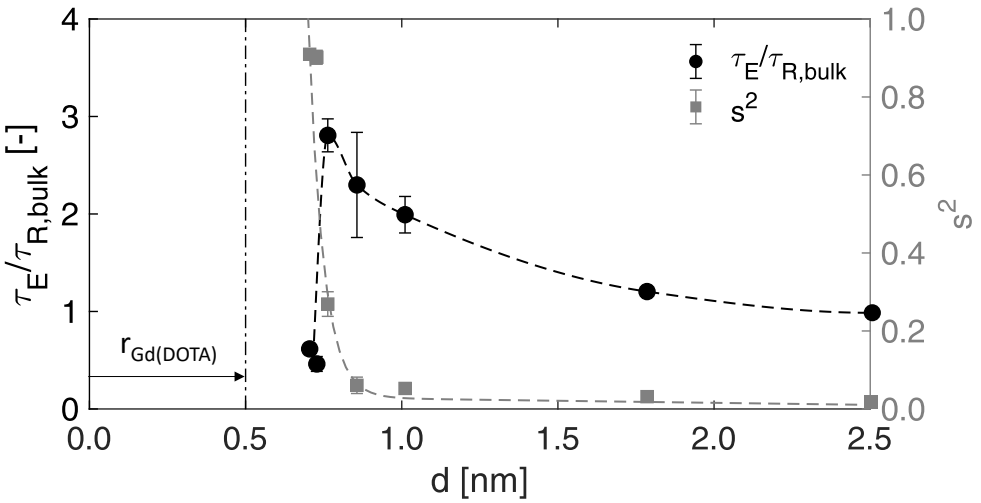

Fig. 3 Trend of the ratio between τ_E (extra correlation time of Gd(DOTA) bonded to a silica wall) and $\tau_{R,bulk} = 75$ ps (tumbling time of Gd(DOTA) complex in bulk water), according to different distances between Gd(DOTA) and silica wall. Trend of S^2 (order parameter) is also shown. The definition of d and $r_{Gd(DOTA)}$ is depicted in Figure 1d. Error bars refer to ± 1 s.d.

Once the autocorrelation function $C_i(t)$ is computed for each trajectory, it is then further averaged among the number of independent repetitions per case and the tumbling time finally obtained from the best fit of the Lipari-Szabo model. The complete details of the considered configurations, including the number of simulation repetitions per case, and the number of time intervals for the integration are reported in the ESI†, S1.

In case of Gd(DOTA) immersed in bulk water (Figure 1a), the obtained $C(t)$ for one run reveals that the molecule experiences a free tumbling motion (Figure 2a, red line); therefore, Equation 2 can be used to compute the characteristic tumbling time τ_R with excellent fitting accuracy (R^2=0.99). In the case of Gd(DOTA) bonded to the silica wall, instead, the tumbling motion is limited by the presence of the silica slab; therefore, the $C(t)$ for one run is now fitted by Equation 3 (Figure 2a and 2b), allowing to extract both the extra correlation time τ_E and the order parameter S^2 with good fitting accuracy (R^2>0.85). Note that, the simulation runs are extended until the simulation time is at least 20 times larger than the characteristic τ_R or τ_E in the considered setup.

The characteristic tumbling time of Gd(DOTA) in water obtained from the current simulations is equal to $\tau_R = \tau_{R,bulk} = 75$ ps at 300 K, being well validated against experimental measures in the literature (77 ± 4 ps at 298 K[48]). When the Gd(DOTA) is bonded to the solid wall, instead, the complex becomes part of a much larger system. In this case, Gd(DOTA) has a constrained tumbling motion, and the RACFs eventually decay to some static value, depending on the tightness of the bonding constraint.[49] The tumbling motion is now characterized by both the order parameter S^2 and the extra correlation time τ_E. Figure 3 presents the results of the 7 tested configurations. The results show that the characteristic tumbling motion is strongly dependent on d, and three different behaviors can be observed over the investigated range of Gd(DOTA)-wall distances. First, the tumbling motion of the bonded Gd(DOTA) resembles the bulk one for $d > 2$ nm, *i.e.* $S^2 \to 0$ and $\tau_E \cong \tau_{R,bulk}$, meaning that Gd(DOTA) and wall motions are completely decoupled and bulk conditions of water are experienced by the molecule. Second, the tumbling motion of Gd(DOTA) is slowed down for $0.7 \text{ nm} < d < 2$ nm, and $\tau_E/\tau_{R,bulk}$ eventually reaches a maximum at $d \cong 0.8$ nm, meaning that the Gd(DOTA) tumbling is significantly affected by the reduced water mobility in the proximity of the silica wall, whereas the Gd(DOTA) and the wall motions are still decoupled (*i.e.* $S^2 \cong 0$). Third, $\tau_E/\tau_{R,bulk}$ undergoes a sharp drop for $d < 0.7$ nm, while S^2 sharply increases. This latter behavior can be interpreted as a progressive full coupling of the Gd(DOTA) and silica wall motions: below $d_{min} \cong 2.5$ Å, the Gd(DOTA) is completely adsorbed and seized by the wall, thus the measured tumbling motion is no more dictated by the surrounding water mobility but is mainly affected by the fast bond oscillations of the Gd-coordination sphere vectors.

Effective water self-diffusivity

The self-diffusion coefficient of water progressively reduces while approaching solid surfaces at the nanoscale.[50,51] This local modification is to be ascribed to the layering and reduced mobility that water molecules experience in the proximity of solid-liquid interfaces with respect to bulk conditions, due to attractive nonbonded interactions.[52,53] In isothermal conditions, the self-diffusion coefficient of water has been numerically and experimentally demonstrated to scale as[3,54,55]

$$D \cong D_B(1-\theta), \tag{9}$$

where D_B is the bulk value and θ is a scaling parameter, defined as the ratio between the nanoconfined and total water volume in the considered configuration, which is representative of the confining

geometry and of the chemistry of the solid surface. The nanoconfined water volume, indeed, is defined as the solvent accessible surface (*SAS*) times a characteristic distance (δ) below which the potential well generated by the solid surface significantly reduce the mobility of the water molecules.[3] The previous equation can be used to estimate the local self-diffusivity as

$$D(z) \cong D_B(1-\theta(z)), \tag{10}$$

where z is the normal coordinate with respect to the considered solid surface (Figure 1d). Equation 10 relates the effective self-diffusivity of the water molecules with the bulk value and with the distance from the solid surface. If the value of $D(d)$ in correspondence of the barycenter of the Gd(DOTA) complex is considered as effective for the whole molecule, then an estimate of the local self-diffusion as a function of the Gd(DOTA)-wall distance can be straightforwardly obtained. However, when the Gd(DOTA) approaches subnanometer distances to the silica surface, D strongly decreases and the latter approximation is no more accurate enough. Then, the effective self-diffusivity of water experienced by the Gd(DOTA) complex in the proximity of the solid surface can be better estimated as:

$$\begin{aligned} D_{\text{eff}} &= \frac{1}{2r_{Gd(DOTA)}}\int_{d_{min}}^{d_{min}+2r_{Gd(DOTA)}} D_B\left(1-\frac{\delta}{z}\right)dz \\ &= D_B\left[1-\frac{\delta}{2r_{Gd(DOTA)}}\ln\left(\frac{d_{min}+2r_{Gd(DOTA)}}{d_{min}}\right)\right], \end{aligned} \tag{11}$$

which is particularly suitable at sub-nanometer distances from the wall (see ESI†, S3 and S4).

Therefore, it is now possible to define an effective distance d_D such that $D_{\text{eff}} = D(d_D)$:

$$d_D = \frac{2r_{Gd(DOTA)}}{\ln\left(\frac{d_{min}+2r_{Gd(DOTA)}}{d_{min}}\right)}, \tag{12}$$

which can be considered as the normal distance between the solid surface and Gd(DOTA) where the self-diffusivity of water predicted by Equation 10 represents the average value experienced overall by Gd(DOTA). Note that the discrepancy between d and d_D, therefore between $D(d)$ and $D(d_D)$, is larger at subnanometer distances from the wall, where water mobility sharply decreases toward near-zero values.

Discussion

Mechanistic modeling of the tumbling motion

In the Lipari-Szapo formalism, the tumbling motion of Gd(DOTA) bonded to a solid wall (Equation 3) is described by the extra correlation time τ_E, which quantifies the actual rotational mobility of the molecule, and by the order parameter S^2. In particular, $S^2 = 1$ if the motion of Gd(DOTA) and of the solid wall are fully coupled by a rigid bond, whereas $S^2 = 0$ implies that the Gd(DOTA) rotational motion is not affected by the wall. Hence, we propose to model the resulting rotational motion of Gd(DOTA) bonded to the wall as a combination of two terms coupled with the order parameter S^2, namely

$$\tau_E(z) = S^2\,\tau_{R,w} + \left(1-S^2\right)\tau_{R,p}(z), \tag{13}$$

where $\tau_{R,w}$ is the tumbling time of Gd(DOTA) seized on the silica wall, $\tau_{R,p}(z)$ is the characteristic tumbling time of Gd(DOTA) if a free motion is considered, and z is the reference coordinate normal to the solid wall (see Figure 1d). In the considered simulation domain (see Figure 1b), the silica wall is restrained in the center of the simulation box. Therefore, when Gd(DOTA) is completely adsorbed on the wall surface, only fast local bond oscillations of the Gd-coordination sphere interacting with the steady wall are allowed, which are in the order of $\tau_{R,w} \cong 1$ ps. On the other hand, the characteristic tumbling time of Gd(DOTA), $\tau_{R,p}(z)$, can be correlated with the mobility of the local surrounding water as:[21]

$$\tau_{R,p}(z) = \frac{1}{6D_{R,p}(z)}, \tag{14}$$

$$D_{R,p}(z) = \frac{k_B T}{8\pi\,\mu(z)\,r^3_{Gd(DOTA)}}, \tag{15}$$

where $D_{R,p}$ is the rotational diffusion coefficient of the spherical shaped Gd(DOTA) in a surrounding medium with viscosity $\mu(z)$, which is affected in turn by the confinement exerted by silica wall on the water molecules in the proximity of its surface. Note that, if bulk conditions of water are recovered, $\tau_{R,p}(z=\infty) = \tau_{R,bulk}$, $S^2 \to 0$ and thus $\tau_E(z=\infty) = \tau_{R,bulk}$.

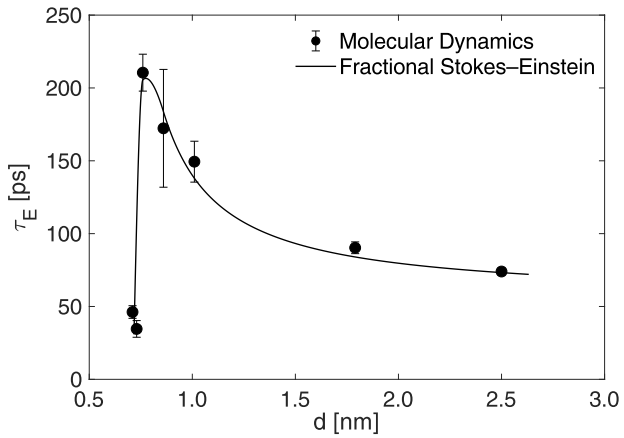

Fig. 4 Extra correlation time τ_E for Gd(DOTA) bonded to a silica wall and located at different normal distances d from the wall surface. Results obtained from MD simulations (dots) and predicted by Equation 13 (solid line) are compared ($R^2 = 0.98$). Error bars refer to ± 1 s.d.

According to the classical Stokes-Einstein relation, the self-diffusivity and viscosity of water are inversely proportional at a given temperature; however, it has been demonstrated that supercooled water violates such a relation.[56–60] In fact, the Stokes-Einstein relation $D \sim \mu^{-1}$ should be replaced by a "Fractional Stokes-Einstein relation" $D \sim \mu^{-k}$ for supercooled water, being $k \leq 1$ a characteristic parameter of the medium.[61] Given the similarities between the transport properties of supercooled and nanoconfined water discussed in Reference[3], the self-diffusivity

and viscosity of water in the proximity of a solid surface can be related as

$$\frac{\mu(z)}{\mu_B} \sim \left(\frac{D(z)}{D_B}\right)^{-1/k}, \tag{16}$$

where μ_B is the dynamic viscosity of bulk water. Recalling Equation 10, $\mu(z)$ could then be expressed in explicit form as

$$\mu(z) \cong \mu_B(1-\theta(z))^{-1/k}. \tag{17}$$

In the case of water molecules confined by a silica wall, Equation 17 becomes

$$\mu(z) \cong \mu_B\left(1-\frac{\delta}{z}\right)^{-1/k}, \tag{18}$$

where $\delta = 0.33$ nm[3] is the characteristic length of water nanoconfinement by a flat surface made of silica with surface silanols. The quantification of $\theta(z)$ for Gd(DOTA) bonded to cylindrical silica nanopores or particles are also discussed in the ESI†, S5.

Notice that the Fractional Stokes-Einstein relation is not the only one correlating the molecular diffusion coefficient with the viscosity of fluids under extreme conditions, but alternative approaches are also available in the literature. For instance, Saugey and co-workers[62] reported approximate forms for the friction factor as function of the fluid confinement, slip length and size of the particles. Such approach is based on the classical hydrodynamic theory, and the analytical forms – which are derived by implementing the iterative reflection method[63] – reproduce quite well the trends of numerical computations in term of translational diffusion coefficient.[62]

For a fair comparison with simulations, the average self-diffusivity acting on the Gd(DOTA) surface has to be considered, *i.e.* the reference system for the MD results has to be transformed as $\tau_E(z=d_D) \rightarrow \tau_E(z=d)$, which from Equation 12 yields:

$$d = \frac{2r_{Gd(DOTA)}}{\exp\left(\frac{2r_{Gd(DOTA)}}{d_D}\right)-1} + r_{Gd(DOTA)}. \tag{19}$$

In the simulated configurations, the Gd(DOTA) complex is solvated using the TIP3P water model, therefore $\mu_B \cong 0.43$ Pa s,[64] $D_B \cong 5.88\times10^{-9}$m^{2}s^{-1}, $T = 300$ K and $r_{Gd(DOTA)} \cong 0.50$ nm.[21] Once $k = 0.46$ is calibrated by best fitting, the results obtained from the MD simulations and Equation 13 are compared in Figure 4, where an excellent agreement ($R^2 = 0.98$) between simulations and modeling predictions for τ_E is found. Notice that the optimized k found for this model is not far from previous evidence in the literature, where values around 0.6 have been reported for supercooled fluids.[61,65–68]

Confinement effect on relaxivity

SBM equations – with input parameters also taken from the MD results and theoretical considerations reported in the previous Sections – are finally employed to predict the Nuclear Magnetic Relaxation Dispersion (NMRD) profiles of the nanoconfined Gd(DOTA) complexes experimentally tested in Reference.[23] In case of Gd(DOTA) bonded to silicon-based particles, the molecular motion of the complex is described by either SiP or SiMP motion, whereas the local motion is due to Gd(DOTA) (see ESI†, S6 and S7 for a detailed description of SBM model).

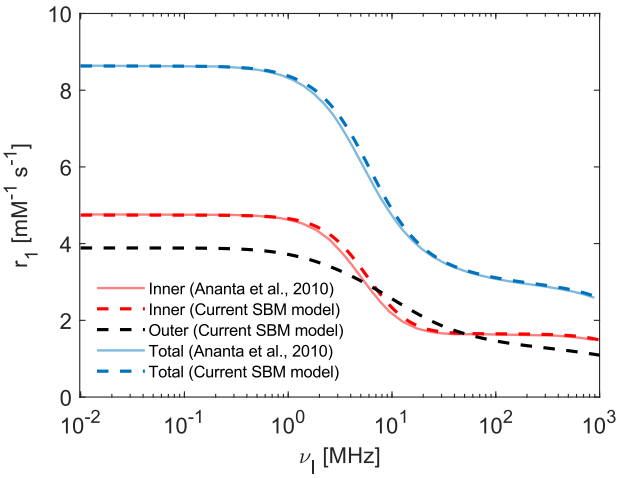

Fig. 5 Validation of the current SBM model for free Gd(DOTA) complex solvated in bulk water, at temperature equal to 310 K. The inner (red) and outer (black) sphere contributions to the total relaxivity (blue) are shown. The current SBM model (dashed lines) show good agreement with previous results (solid lines) reported by Ananta *et al.*[21]

After validating the current implementation of the SBM model against previously reported data[21] for the case of free Gd(DOTA) complex solvated in bulk water (see the NMRD profiles in Fig. 5, and the details of the reference test case reported in ESI†, S8), the NMRD profiles for Gd(DOTA) bonded to SiP are computed. The minimum distance between DOTA and SiP surface (d_{min}) is varied over the range 0.22–2 nm, and the corresponding family of NMRD profiles is reported in Figure 6. Considering the clinically relevant frequencies tested in the experiments (60 MHz), the longitudinal relaxivity value measured by Gizzatov *et al.*[23] for the Gd(DOTA)+SiP complex (r_1=8.09 ± 2.1 mM^{-1}s^{-1}) is recovered for models with d_{min} between 0.26 and 0.55 nm. These values are coherent with the average relative distance between Gd(DOTA) and the solid wall that should be achieved with the 1-nm long APTES chains adopted in the experiments ($d_{min} \approx 0.55$ nm for $b \approx 1$ nm,[23] see ESI†, S3). Further comparison between model and experimental values are reported in the ESI†, S9. Overall, the model predictions show that the relaxivity is significantly enhanced when a strong coupling (*i.e.* $S^2 \rightarrow 1$) between the Gd(DOTA) and SiP is achieved; whereas the NMRD profile of the pure Gd(DOTA) is progressively recovered at larger distances (*i.e.* decoupling) between the Gd chelate and the silica surface. Even though τ_E of the Gd(DOTA) sharply decreases at $d_{min} < 0.26$ nm (Figure 3), r_1 increases anyway, because the increase in both S^2 and τ_D while approaching the SiP surface are the prevailing effects, which eventually enhance the Gd(DOTA) relaxivity. Hence, the relaxivity enhancement observed in Reference[23] may be attributed to the synergistic contribution of the Paramagnetic Relaxation Enhancement – PRE effect[17] (due to the Gd(DOTA) complex adsorption to the pore walls of a micrometer particle) and of the increase in the diffusion correlation times (induced by the reduced mobility of the water molecules in the proximity of solid surfaces), as the pore sizes decreases. There-

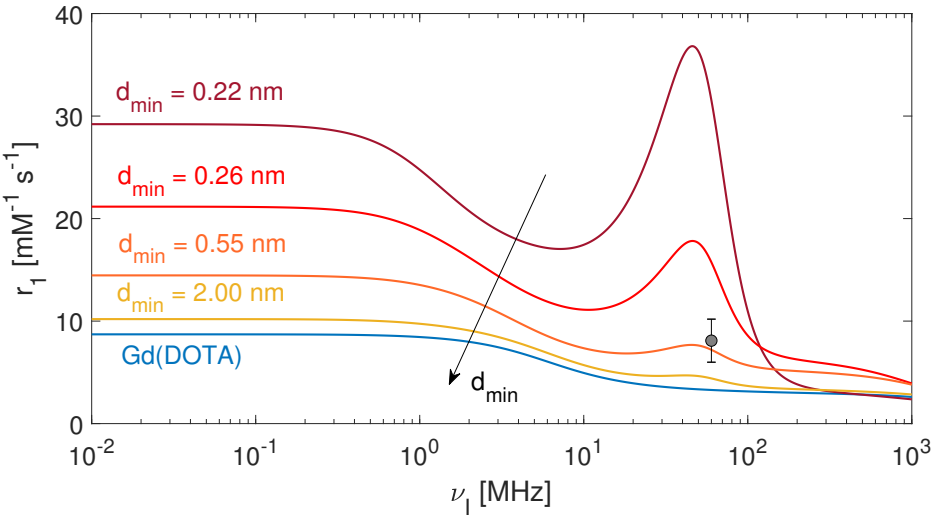

Fig. 6 NMRD profiles of Gd(DOTA) and Gd(DOTA) bonded to SiP, according to different d_{min}. The predicted values of r_1(1.41 T) at clinically relevant frequencies (60 MHz) are the following: 31.3 $mM^{-1}s^{-1}$ ($d_{min} = 0.22$ nm); 15.5 $mM^{-1}s^{-1}$ ($d_{min} = 0.26$ nm); 7.0 $mM^{-1}s^{-1}$ ($d_{min} = 0.55$ nm); 4.2 $mM^{-1}s^{-1}$ ($d_{min} = 2.0$ nm). Note that $r_1(1.41\ T) = 8.09 \pm 2.1\ mM^{-1}s^{-1}$ in the experiments, which is represented by the gray circle.[23]

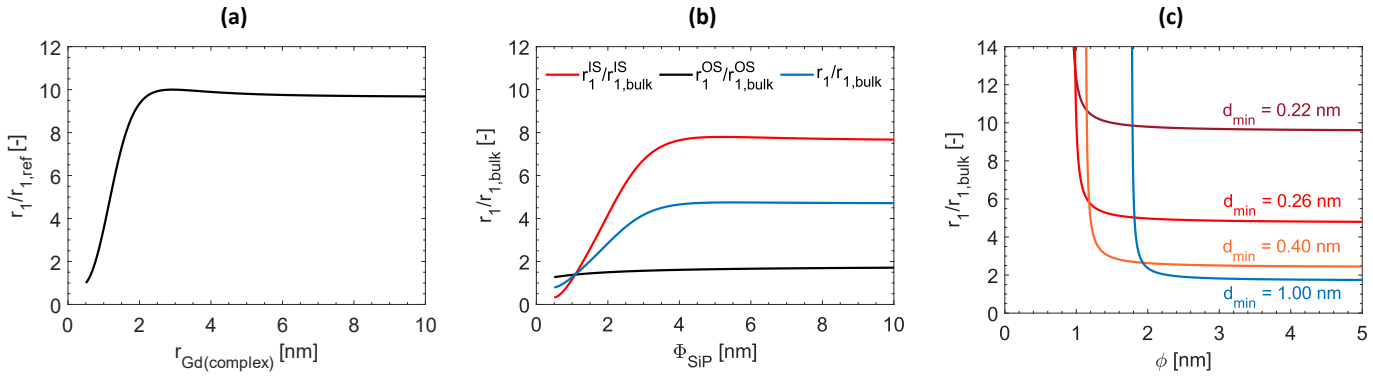

Fig. 7 Parametric analysis of the r_1 relaxivity at 1.41 T for: (a) Gd-based complexes with increasing radius $r_{Gd(complex)}$. Values are normalized by the reference relaxivity of Gd(DOTA) at 1.41 T. (b) Gd(DOTA)-SiP complexes with increasing SiP diameter (Φ_{SiP}): inner sphere (IS, red line), outer sphere (OS, black line) and total (blue line) relaxivities are shown. Values are normalized by the corresponding relaxivities of Gd(DOTA) immersed in bulk water. (c) Gd(DOTA)-SiMP complexes with increasing pore diameter (ϕ) and minimum DOTA-surface distance (d_{min}). Values are normalized by the corresponding relaxivity of Gd(DOTA) immersed in bulk water.

fore, the geometrical confinement of Gd(DOTA) both limits its free tumbling (inner-sphere effect) and the diffusion of the surrounding water molecules (outer-sphere effect), which are then forced to interact longer with the paramagnetic agent adsorbed to the inner pore surface.[21,69]

Finally, we analyze the r_1 relaxivity for different characteristics of the paramagnetic complex and of the confining particle. In particular, we systematically analyze the effect of (i) Gd-based complex size, (ii) SiP diameter in Gd(DOTA)+SiP complexes and (iii) SiMP pore diameter in Gd(DOTA)+SiMP complexes. The results of the parametric analysis are reported in Figure 7. First, Figure 7(a) shows that an increasing radius of possible Gd-based complexes alternative to DOTA may have a beneficial effect on clinically relevant relaxivities, due to increased τ_R (see ESI†, S10). However, a plateau is reached for $r_{Gd(complex)} \cong 2$ nm; thus, further increases seem to have no significant effect on r_1. Second, Figure 7(b) shows that the relaxivity of Gd(DOTA)+SiP complexes may be enhanced by larger SiP diameters (or increasing the coupling between Gd(DOTA) and SiP motion, *i.e.* $S^2 \to 1$, see ESI†, S10). In this case, the inner sphere contribution plays the major role on the overall relaxivity enhancement; however, while the molecular tumbling time of SiP increases with its diameter, a plateau of $1/T_{1m}$ (and thus of r_1^{IS}) is reached with $\Phi_{SiP} \cong 4$ nm (see ESI†, S10). Then, further increase of the diameter beyond this value seem to have no significant effect on r_1. Finally, the curves in Figure 7(c) demonstrate that sharp relaxivity enhancements for Gd(DOTA)+SiMP complexes may be achieved by either reducing the nanopore width or by approaching the Gd(DOTA) to the pore surface.

Summary and conclusions

We have analyzed the effect of confinement of water molecules on the behavior of paramagnetic colloidal complexes, which are typically adopted as contrast agents in magnetic resonance imaging. Based on atomistic simulations, the tumbling and diffusion times of the gadolinium-based complex Gd(DOTA) have been examined in bulk and confined conditions, and a mechanistic model for the interpretation of the results in the light of the mobility reduction of water molecules in the proximity of solid surfaces has been proposed. The experimental set-up reported in Reference [23] has been adopted, and the related nanoconstructs have been mimicked by Gd(DOTA) complex bonded to silica walls. The bulk tumbling time of the complex has been found to accurately match the experiments. The tumbling time of the confined complex, which depends on its distance from the wall, has been interpreted in the light of the Lipari-Szabo formalism (see ESI†, S11 for a discussion on the applicability of this model-free approach) and of the local modification of solvent properties, based on the fractional Stokes-Einstein relation for estimating the local water viscosity. This latter scaling has been related to the effect of local confinement of the water molecules using a previously reported expression for the self-diffusion of water under nanoconfined conditions.[3]

It has been found that the geometrical confinement of the paramagnetic complex limits its free tumbling on the inner-sphere, and the diffusion of the surrounding water molecules on the outer-sphere. These effects force water molecules to have a longer interaction (resident time) with the paramagnetic agent adsorbed to the inner pore surface. Based on the results obtained, it is suggested that the design of novel nanovectors aiming to enhance the relaxation properties of Gd(DOTA) may encompass the following characteristics (see Figure 7 and ESI†, S10): i) a stiff (*i.e.* high S^2) and short (*i.e.* low d_{min}) bonding chain between the paramagnetic complex and the surface of the nanovector (ideally, a single covalent bond between the DOTA and the nanovector surface may give the largest r_1 enhancement); ii) a diameter of the nanovector smaller than a few tens of nanometers; iii) a microporous structure, with pore diameters typically smaller than 4 nm. As an example, similar features may be found in nanovectors made out of zeolite [70,71] or polymer bundles.[72]

Conflicts of interest

There are no conflicts to declare.

Acknowledgments

The authors acknowledge the computational resources provided by HPC@POLITO (http://www.hpc.polito.it). We thank Paolo Decuzzi for helpful discussions. This article is published online at https://doi.org/10.1039/D1CP00708D.

Author contributions

Luca Bergamasco: Validation, Formal analysis, Writing - Review & Editing, Visualization. Matteo Morciano: Validation, Formal analysis, Writing - Review & Editing, Visualization. Matteo Fasano: Conceptualization, Methodology, Formal analysis, Investigation, Data Curation, Writing - Original Draft, Visualization, Supervision.

Notes and references

1 G. Algara-Siller, O. Lehtinen, F. Wang, R. Nair, U. Kaiser, H. Wu, A. Geim and I. Grigorieva, *Nature*, 2015, **519**, 443–445.
2 S. Zhang, J. Zhang, Y. Zhang and Y. Deng, *Chemical Reviews*, 2017, **117**, 6755–6833.
3 E. Chiavazzo, M. Fasano, P. Asinari and P. Decuzzi, *Nature communications*, 2014, **5**, 4495.
4 M. Neek-Amal, F. Peeters, I. Grigorieva and A. Geim, *ACS Nano*, 2016, **10**, 3685–3692.
5 W. Aftab, X. Huang, W. Wu, Z. Liang, A. Mahmood and R. Zou, *Energy and Environmental Science*, 2018, **11**, 1392–1424.
6 C. Sun, R. Zhou, Z. Zhao and B. Bai, *The Journal of Physical Chemistry Letters*, 2020, **11**, 4678–4692.
7 M. Fasano, G. Falciani, V. Brancato, V. Palomba, P. Asinari, E. Chiavazzo and A. Frazzica, *Applied Thermal Engineering*, 2019, **160**, 114075.
8 M. Fasano, A. Bevilacqua, E. Chiavazzo, T. Humplik and P. Asinari, *Scientific reports*, 2019, **9**, 1–12.
9 P. Malgaretti, I. Pagonabarraga and M. Rubi, *Frontiers in Physics*, 2013, **1**, 21.
10 P. Malgaretti, I. Pagonabarraga and J. M. Rubi, *The European Physical Journal Special Topics*, 2014, **223**, 3295–3309.
11 M. Fasano, T. Humplik, A. Bevilacqua, M. Tsapatsis, E. Chiavazzo, E. N. Wang and P. Asinari, *Nature communications*, 2016, **7**, 1–8.
12 K. Riehemann, S. W. Schneider, T. A. Luger, B. Godin, M. Ferrari and H. Fuchs, *Angewandte Chemie International Edition*, 2009, **48**, 872–897.
13 A. Singhal, J. D. Schneible, R. L. Lilova, C. K. Hall, S. Menegatti and A. Grafmüller, *Soft Matter*, 2020, **16**, 10591–10610.
14 H. S. Sachar, T. H. Pial, B. S. Chava and S. Das, *Soft Matter*, 2020, **16**, 7808–7822.
15 C. M. Lépori, N. M. Correa, J. J. Silber, F. V. Chávez and R. D. Falcone, *Soft Matter*, 2019, **15**, 947–955.
16 S. Aryal, H. Park, J. F. Leary and J. Key, *International journal of nanomedicine*, 2019, **14**, 6631.
17 R. B. Lauffer, *Chemical Reviews*, 1987, **87**, 901–927.
18 C. Sun, J. S. Lee and M. Zhang, *Advanced drug delivery reviews*, 2008, **60**, 1252–1265.
19 P. Caravan, *Chemical Society Reviews*, 2006, **35**, 512–523.
20 S. Tong, S. Hou, Z. Zheng, J. Zhou and G. Bao, *Nano letters*, 2010, **10**, 4607–4613.
21 J. S. Ananta, B. Godin, R. Sethi, L. Moriggi, X. Liu, R. E. Serda, R. Krishnamurthy, R. Muthupillai, R. D. Bolskar, L. Helm *et al.*, *Nature nanotechnology*, 2010, **5**, 815–821.
22 Z. Zhou, L. Yang, J. Gao and X. Chen, *Advanced Materials*, 2019, **31**, 1804567.
23 A. Gizzatov, C. Stigliano, J. S. Ananta, R. Sethi, R. Xu, A. Guven, M. Ramirez, H. Shen, A. Sood and M. Ferrari, *Cancer letters*, 2014, **352**, 97–101.

24 C. A. Chang, L. C. Francesconi, M. F. Malley, K. Kumar, J. Z. Gougoutas, M. F. Tweedle, D. W. Lee and L. J. Wilson, *Inorganic Chemistry*, 1993, **32**, 3501–3508.

25 F. Yerly, K. I. Hardcastle, L. Helm, S. Aime, M. Botta and A. E. Merbach, *Chemistry-A European Journal*, 2002, **8**, 1031–1039.

26 K. Kihara, *European Journal of Mineralogy*, 1990, **2**, 63–77.

27 W. L. Jorgensen, D. S. Maxwell and J. Tirado-Rives, *Journal of the American Chemical Society*, 1996, **118**, 11225–11236.

28 W. L. Jorgensen, J. Chandrasekhar, J. D. Madura, R. W. Impey and M. L. Klein, *The Journal of Chemical Physics*, 1983, **79**, 926–935.

29 A. Borel, L. Helm and A. E. Merbach, *Chemistry-A European Journal*, 2001, **7**, 600–610.

30 P. E. Lopes, V. Murashov, M. Tazi, E. Demchuk and A. D. MacKerell, *The Journal of Physical Chemistry B*, 2006, **110**, 2782–2792.

31 S. J. Weiner, P. A. Kollman, D. T. Nguyen and D. A. Case, *Journal of Computational Chemistry*, 1986, **7**, 230–252.

32 A. Malani, K. Ayappa and S. Murad, *The Journal of Physical Chemistry B*, 2009, **113**, 13825–13839.

33 F. Yerly, A. Borel, L. Helm and A. E. Merbach, *Chemistry-A European Journal*, 2003, **9**, 5468–5480.

34 B. Hess, C. Kutzner, D. Van Der Spoel and E. Lindahl, *Journal of chemical theory and computation*, 2008, **4**, 435–447.

35 H. Chávez Thielemann, A. Cardellini, M. Fasano, L. Bergamasco, M. Alberghini, G. Ciorra, E. Chiavazzo and P. Asinari, *Journal of Molecular Modeling*, 2019, **25**, 147.

36 E. F. Pettersen, T. D. Goddard, C. C. Huang, G. S. Couch, D. M. Greenblatt, E. C. Meng and T. E. Ferrin, *Journal of Computational Chemistry*, 2004, **25**, 1605–1612.

37 M. P. Allen and D. J. Tildesley, *Computer simulation of liquids*, Oxford university press, 1989.

38 H. J. Berendsen, J. P. M. Postma, W. F. van Gunsteren, A. DiNola and J. Haak, *The Journal of chemical physics*, 1984, **81**, 3684–3690.

39 S. Nosé, *The Journal of Chemical Physics*, 1984, **81**, 511–519.

40 W. G. Hoover, *Physical Review A*, 1985, **31**, 1695–1697.

41 M. Parrinello and A. Rahman, *Journal of Applied physics*, 1981, **52**, 7182–7190.

42 G. Lipari and A. Szabo, *Journal of the American Chemical Society*, 1982, **104**, 4546–4559.

43 A. Villa and G. Stock, *Journal of chemical theory and computation*, 2006, **2**, 1228–1236.

44 E. A. Cino, M. Karttunen and W.-Y. Choy, *PloS one*, 2012, **7**, e49876.

45 N. Tjandra, S. E. Feller, R. W. Pastor and A. Bax, *Journal of the American Chemical Society*, 1995, **117**, 12562–12566.

46 G. M. Nicolle, E. Toth, H. Schmitt-Willich, B. Raduchel and A. E. Merbach, *Chemistry-A European Journal*, 2002, **8**, 1040–1048.

47 K. K. Frederick, K. A. Sharp, N. Warischalk and A. J. Wand, *The Journal of Physical Chemistry B*, 2008, **112**, 12095–12103.

48 D. H. Powell, O. M. N. Dhubhghaill, D. Pubanz, L. Helm, Y. S. Lebedev, W. Schlaepfer and A. E. Merbach, *Journal of the American Chemical Society*, 1996, **118**, 9333–9346.

49 P. Caravan, C. T. Farrar, L. Frullano and R. Uppal, *Contrast media and molecular imaging*, 2009, **4**, 89–100.

50 S. Romero-Vargas Castrillon, N. Giovambattista, I. A. Aksay and P. G. Debenedetti, *The Journal of Physical Chemistry B*, 2009, **113**, 7973–7976.

51 K. Tankeshwar and S. Srivastava, *Nanotechnology*, 2007, **18**, 485714.

52 L. Bergamasco, M. Alberghini and M. Fasano, *Nanoscale research letters*, 2019, **14**, 1–11.

53 P. Gallo, M. Rovere and E. Spohr, *Physical review letters*, 2000, **85**, 4317.

54 S. O. Diallo, *Physical Review E*, 2015, **92**, 012312.

55 N. C. Osti, A. Cote, E. Mamontov, A. Ramirez-Cuesta, D. Wesolowski and S. Diallo, *Chemical Physics*, 2016, **465**, 1–8.

56 S.-H. Chen, F. Mallamace, C.-Y. Mou, M. Broccio, C. Corsaro, A. Faraone and L. Liu, *Proceedings of the National Academy of Sciences*, 2006, **103**, 12974–12978.

57 S. R. Becker, P. H. Poole and F. W. Starr, *Physical review letters*, 2006, **97**, 055901.

58 M. G. Mazza, N. Giovambattista, H. E. Stanley and F. W. Starr, *Physical Review E*, 2007, **76**, 031203.

59 F. Fernandez-Alonso, F. Bermejo, S. McLain, J. Turner, J. Molaison and K. Herwig, *Physical review letters*, 2007, **98**, 077801.

60 T. Kawasaki and K. Kim, *Scientific reports*, 2019, **9**, 1–9.

61 L. Xu, F. Mallamace, Z. Yan, F. W. Starr, S. V. Buldyrev and H. E. Stanley, *Nature Physics*, 2009, **5**, 565–569.

62 A. Saugey, L. Joly, C. Ybert, J.-L. Barrat and L. Bocquet, *Journal of Physics: Condensed Matter*, 2005, **17**, S4075.

63 J. Happel and H. Brenner, *Low Reynolds number hydrodynamics: with special applications to particulate media*, Springer Science & Business Media, 2012, vol. 1.

64 M. Lai, M. Kalweit and D. Drikakis, *Molecular Simulation*, 2010, **36**, 801–804.

65 J. Douglas and D. Leporini, *Journal of non-crystalline solids*, 1998, **235**, 137–141.

66 K. R. Harris, *Communications: The fractional Stokes–Einstein equation: Application to water*, 2010.

67 B. P. Bhowmik, R. Das and S. Karmakar, *Journal of Statistical Mechanics: Theory and Experiment*, 2016, **2016**, 074003.

68 S.-W. Choi, S. Kim and Y. Jung, *The Journal of chemical physics*, 2015, **142**, 244506.

69 R. Sethi, J. S. Ananta, C. Karmonik, M. Zhong, S. H. Fung, X. Liu, K. Li, M. Ferrari, L. J. Wilson and P. Decuzzi, *Contrast media and molecular imaging*, 2012, **7**, 501–508.

70 H. Lulf, A. Bertucci, D. Septiadi, R. Corradini and L. De Cola, *Chemistry-A European Journal*, 2014, **20**, 10900–10904.

71 A. Bertucci, H. Lülf, D. Septiadi, A. Manicardi, R. Corradini and L. De Cola, *Advanced healthcare materials*, 2014, **3**, 1812–1817.

72 J. Key, S. Aryal, F. Gentile, J. S. Ananta, M. Zhong, M. D. Landis and P. Decuzzi, *Biomaterials*, 2013, **34**, 5402–5410.